A Deep Learning Approach for Classification of Reaching Targets from EEG Images

Schubert R. Carvalho*¶, Iraquitan C. Filho*, Damares O. Resende*, Ana C. Siravenha*, Cleidson R. B. de Souza*
Henrique Debarba†§, Bruno D. Gomes*‡ and Ronan Boulic§
Laboratório de Computação Aplicada*, Instituto Tecnológico Vale (ITV), Brazil
Instituto de Ciências Biológicas‡, Universidade Federal do Pará (UFPA), Brazil
Artanim Foundation†, Switzerland
Immersive Interaction Group (IIG)§ École polytechnique fédérale de Lausanne (EPFL), Switzerland
schubert.carvalho@itv.org¶

***Abstract*—In this paper, we propose a new approach for the classification of reaching targets before movement onset, during visually-guided reaching in 3D space. Our approach combines the discriminant power of two-dimensional Electroencephalography (EEG) signals (i.e., EEG images) built from short epochs, with the feature extraction and classification capabilities of deep learning (DL) techniques, such as the Convolutional Neural Networks (CNN). In this work, reaching motions are performed into four directions: left, right, up and down. To allow more natural reaching movements, we explore the use of Virtual Reality (VR) to build an experimental setup that allows the subject to perform self-paced reaching in 3D space while standing. Our results reported an increase both in classification performance and early detection in the majority of our experiments. To our knowledge this is the first time that EEG images and CNN are combined for the classification of reaching targets before movement onset.**

I. Introduction

In the last ten years, research combining Virtual Reality (VR) and Brain-Computer Interfaces (BCI) from Electroencephalography (EEG) of brain activity has increased [1]–[3]. One reason is that, VR provides a safe and controlled test environment for the development of BCI-VR applications. For example, the classification of reaching targets from (EEG) signals before movement onset, which has important applications in the area of neuro-prostheses control [4].

Research in BCI for reaching can be broadly divided into two groups 1) classification of reaching targets as quickly and accurately as possible 2) reconstruction of arm trajectories. In this work, we propose a solution for the former problem, that handles visually-guided reaching in three-dimensional (3D) space. In visually-guided reaching in 3D space, it is believed that the brain converts visual signals into a motor plan to drive the arm towards the target [5]. This type self-paced reaching is challenge to decode because the subject decides when and how he/she will produce the movement towards the target. Moreover, the classification of reaching targets from EEG signals is still harder, because of the non-stationary characteristics of these these signals - that can be decomposed and analyzed in different frequency bands or components - its high variability across target selections and its low signal to noisy ratio. All of these issues together contribute to low classification performances.

It is well known that EEG frequency bands can correlate with the cognitive task being performed [6], [7]. For instance, the execution and intention of motor actions modulates μ and δ rhythms, respectively [4], [8]. These two frequency ranges are classically defined as $(8-13)$Hz and $(0-4)$Hz, respectively. It has been reported that EEG amplitudes (in μV) extracted from uni-dimensional (1D) sub-ranges of the δ band, encapsulates anticipatory patterns that can be used to classify reaching direction before movement onset [4]. In order to increase the pattern space of feasible targets, we explore the use of bi-dimensional (2D) patterns (i.e., images) drawn up from one-dimensional (1D) EEG, to classify reaching targets in 3D space before the movement is initiated. To handle EEG images we explore the use of deep learning (DL) techniques.

Deep learning is a classification method that handles the type of data encapsulated within EEG images. The non-stationary characteristics of EEG recordings present a wide variation in time, space and across subjects. Such complex and multilevel variations are prone to be analyzed with a multilevel hierarchically organized classifiers. Despite just a few studies using DL for EEG pattern classification are available, there is clearly an increased tendency of using such techniques to achieve better results using deep neural networks (DNN) architectures when compared to other classifiers such as support vector machines (SVMs).

In [9] a CNN architecture whose topology consisted of two convolution layers was used to classify the presence of the P300 in the EEG, while subjects were required to identify a character contained in a 6×6 matrix. Their result showed a high classification accuracy with 8 out of 64 channels. In [10] was evaluated a deep architecture for motor imagery classification where the hidden layers were explicitly represented by combining pre-trained hidden layers with a later use of AdaBoost algorithm. In this approach the authors were able to show a better classification result compared to SVM classifiers despite a strong variability across subjects. In [11] motor imagery classification was investigated with three variations of a deep architecture. Best accuracy results and less inter

subject variation was accomplished using a combination of CNNs with stacked auto encoders.

In this study, we propose a new approach for classification of reaching targets before movement onset. Our approach combines the discriminant power of EEG images built from short epochs of 250ms, with the feature extraction capabilities of a deep learning technique called Convolutional Neural Network (CNN), which is suitable to learn patterns directly from image data and flexible enough to overcome local distortions. We then use a sliding window technique to continuously classify the intended target during the intention period (intention is considered as the cognitive state that leads to specific actions before the movement initiates). This allow us to visualize the temporal classification evolution of visually-guided reaching in 3D space before movement onset. Overall, we aim to use a DL approach to investigate the feasibility of classifying reaching targets before movement onset in a VR environment. To our knowledge this is the first time DL is used for this purpose. We demonstrate the performance of our approach in several situations, as described in Section III.

II. Materials and Methods

A. Data Recording Setup

Motion capture (Mocap) and EEG data were recorded from a healthy right-handed male subject. The task consisted in performing a full-body goal-directed reaching with his dominant arm towards one of seven targets within a 3-dimensional (3D) virtual reality (VR) environment as shown in Figure 1. In our VR self-paced protocol, the subject decided the time to start the movement and the target to reach.

The virtual scene consisted of a room measuring $(3\text{m} \times 3\text{m} \times 2.7\text{m})$. A virtual tennis ball was used as a target. The rationale here was that by showing a familiar object the subject comprehends better the scale and dimensions of the virtual scene. After every reach the subject had to return his hand to a resting position represented by a blue sphere placed at the right side of the virtual body waist (Figure 1b). In order to provide a collision feedback to the subject, the resting position and target spheres changed color whenever the subject touched them to indicate a task accomplishment. Finally, a virtual mirror was placed in front of the subject to reinforce the self awareness of the virtual body and compensate for the limited field of view (FoV) the Oculus DK2 offers (around 90 degrees in practice). To account for size variability between the subject and the virtual human bodies a calibration step was performed based on a standard T-posture. The calibration allows the virtual body to follow the subject's movements. An in-house analytic inverse kinematics (IK) solution was used to animate the virtual body [12]. The virtual environment and the IK solution were implemented as an Unity plug-in. Reaching targets were grouped within four different classes, namely Up (class 1), Down (class 2), Left (class 3), and Right (class 4) targets. Two sessions on 10 consecutive days were recorded. Each session was performed during 10min with a 5min break, yielding a total of 200min recorded Mocap and EEG data. EEG data was recorded at 2048Hz using a wireless

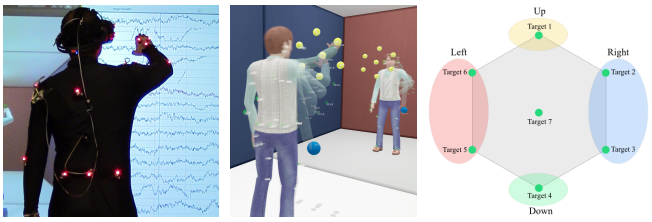

(a) Experimental Setup (b) Virtual scene (c) Reaching targets

Fig. 1. Self-paced goal-directed reaching experimental protocol. Full-body motion capture was recorded in real time. Figure 1a shows the subject using a Mocap suit with 37 LED red marks, an Oculus DK2 for VR immersion and the Emotiv neuroheadset for EEG data recording. Figure 1b shows the virtual body following a subject's reaching motion. Virtual targets are represented by seven yellow tennis balls and a blue ball indicates the resting position. Collision detection algorithms were added to indicate task accomplishment. Figure 1c shows the 4-classes mapping from the seven reaching targets, the middle target was unconsidered.

Emotiv EPOC neuroheadset with 14 channels: $\{AF3,\ F7,\ F3,\ FC5,\ T7,\ P7,\ O1,\ O2,\ P8,\ T8,\ FC6,\ F4,\ F8,\ AF4\}$. Before the neuroheadset sends the EEG signals wirelessly, it filters the signals between 0.2 and 45Hz and down-sample at 128Hz. The open-source software platform OpenVibe [13] was used to record the EEG signals into CSV files. Full-body reaching motions were recorded using a PhaseSpace Impulse X2 Mocap system. 3D locations in Cartesian space of head, torso, shoulder, arms, wrists, hands, legs and feet were sampled at 240Hz. A User Datagram Protocol (UDP) connection was used to trigger the Openvibe and PhaseSpace platforms allowing Mocap and EEG data synchronization.

B. EEG Image Representation

In the current study, as movement intention is related to motor actions, we used channels correspondig to electrodes placed on the frontal lobe $\{F3, F4\}$ and fronto-central lobe $\{FC5, FC6\}$ that capture activity from pre-motor and motor cortex [14]. Amplitude variation in time domain from the δ frequency range was extracted from EEG raw data by filtering with a band-pass zero-phase Butterworth filter. To avoid the ripple side-effect - as a consequence of producing a higher order filter with a steep roll-off [15] - we compute the difference between the highest and lowest cutoff frequencies. If the difference was < 3, then a 3^{rd} order filter was used, otherwise a 4^{th} order was applied. The δ band was then decomposed into 8 frequency ranges for each of the four channels as follows: $\delta_1 = (0.2 - 1\text{ Hz})$, $\delta_2 = (0.2 - 2\text{ Hz})$, $\delta_3 = (0.5 - 1\text{ Hz})$, $\delta_4 = (0.5 - 2\text{ Hz})$, $\delta_5 = (1 - 2\text{ Hz})$, $\delta_6 = (1 - 3\text{ Hz})$, $\delta_7 = (1 - 4\text{ Hz})$, and $\delta_8 = (2 - 4\text{ Hz})$. Finally, EEG images were built concatenating the 8 1D sub-frequency components, as shown by the following array X:

$$\mathrm{X} = \begin{bmatrix} x_{1,\delta_1}^{c_1} & \cdots & x_{1,\delta_1}^{c_k} & \cdots & x_{1,\delta_f}^{c_1} & \cdots & x_{1,\delta_f}^{c_k} \\ \vdots & \ddots & \vdots & & \vdots & \ddots & \vdots \\ x_{j,\delta_1}^{c_1} & \cdots & x_{j,\delta_1}^{c_k} & \cdots & x_{j,\delta_f}^{c_1} & \cdots & x_{j,\delta_f}^{c_k} \\ \vdots & \ddots & \vdots & & \vdots & \ddots & \vdots \\ x_{N,\delta_1}^{c_1} & \cdots & x_{N,\delta_1}^{c_k} & \cdots & x_{N,\delta_f}^{c_1} & \cdots & x_{N,\delta_f}^{c_k} \end{bmatrix}^{\mathrm{T}} \quad (1)$$

Where, N denotes the number of sampled time-points of channel $\{c_k\}_{k=1\ldots4}$, x_{j,δ_f}^{c} is the j^{th} attribute of X at a given frequency range f within the δ band and T indicates the transpose. In the end, each image had a size of 32×32 given a total of 1024 attributes. The matrix X comprised the input image for the deep classifier. Figure 2 depicts the EEG

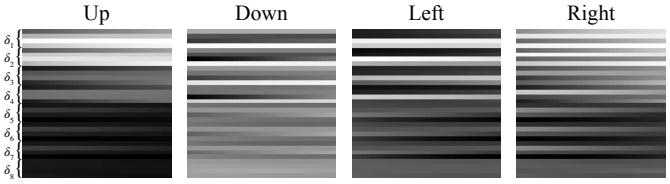

Fig. 2. EEG image patterns for each of the directed-reaching targets.

image in grey contrast for each of the 4-classes generated in this study. Each image in Figure 2 shows an average pattern representation for each of the 4-classes studied (reach directions).

C. Training and Test Datasets

EEG and Mocap were recorded for 10 days, 2 sessions daily, which comprised a total of 2140 trials for the 4 classes. The next step divided the data into training and testing sets. So, 90% of the trials were randomly selected to compose the training set and the remaining trials provided the test set. The training set was composed of images from short epochs [16] of $250\mathrm{ms}$ which corresponded to the intention time interval, that is, a time window prior to the reaching onset within the $[-1s\ 0s]$ interval. The time 0 marked the reaching onset. Epochs were obtained by using a sliding window procedure. To increase the number of training images, epochs were measured with overlapping every $7.8\mathrm{ms}$, yielding a total of 97 epochs per trial. Thus, the training set has a total of 186.822 images. In order to analyze the response of the trained classifiers, the validation model was performed using sliding windows of $250\mathrm{ms}$ within $[-2.5s\ 0s]$ and overlapping every $62.5\mathrm{ms}$. This overlapping adequately encapsulates the variation of δ amplitudes within a $1\mathrm{s}$ time window [17].

D. Deep Learning Approach

We used images to build a pattern space representation of the EEG recordings able to encapsulate the desired information for the subsequent classification. Considering the use of EEG images, we used a deep neural network model, such as the Convolutional Neural Network (CNN), to learn and classify reaching targets. CNN is known to efficiently learn patterns directly from 2D data overcoming important issues that arise when using ordinary fully connected feed-forward networks, such as the pre-processing of the image dimensions. Moreover, CNNs are especially flexible with respect to the variance in translations or local image distortions [18], because of a hierarchical representation that maintains a level of shift, scale, and distortion invariance [19].

The ability of the CNN to learn complex functions that in turn represent complex abstractions from the data lies on how the inputs are transformed throughout the network. Despite of the linear, sigmoidal and hyperbolic tangent are well known functions that increase the features expressiveness, the Rectified Linear Unit (ReLU) function is widely used. Mainly because, the ReLu obtains sparse representations of the data which promotes the information disentangling, efficient variable-size representation, it has other features that resembles the biological information encoding and it provides fast calculations ($ReLU(z) = max(0, z)$) [20]. In addition, CNN suffers less from the vanishing gradient problem [21].

1) CNN Architecture: The CNN architecture is a four-learned layers model: two implement convolution and two fully-connected. Figure 3 shows an illustration of the CNN architecture used in this work. The 32×32 image is presented as the input. It is convoluted with 50 different filters, each of size 11×11, using a stride of one in both width and height, generating 6050 parameters. The resulting feature maps are then passed through a ReLU function, and pooled with overlapping pooling regions (stride of 1) and no-padding.

Similar operations are repeated in layer 2, that is composed of 800 filters of size 5×5 and stride of 1, given a total of 20000 parameters. The feature maps are passed through another ReLU layer and then pooled with overlapping pooling regions (stride of 2) and padding of 1.

The last learner layer is fully connected, taking features from the top convolutional layer as input in vector form. This layer is followed by ReLU and dropout (50%) layers. The final layer is a 4-way softmax function responding the probability distribution of four classes with cross-entropy loss function.

2) Training the CNN Classifiers: The CNN was trained with stochastic gradient descent at an initial learning rate of 0.0001. The learning rate was reduced by 0.1 at each 10 epochs, at a total of 20 epochs (an average of 15 iteration per epoch). The factor for the L2 regularizer is 0.0001 and the batch size for each epoch is 128 with momentum of 0.9. The input data was shuffled once before training and zero-centered every time data is forward-propagated through the input layer. The default initial weights are a Gaussian distribution with mean 0 and standard deviation 0.01, and the default for the initial bias is 0.

Figure 4 presents the first 20 weights of each convolutional layer. The first layer's weights were learned to detect activations along the vertical axis. Some of them respond better to signals in the first channels (row 1, column 8, for example), while the opposite occurs for the last channels (row 2, column 1, for example). Lighter regions correspond

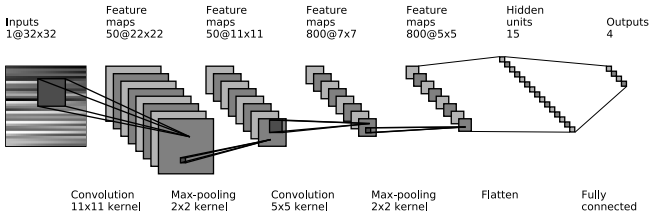

Fig. 3. The CNN architecture is composed of 3 learned layers, max pool and ReLU layers, besides fully-connected and softmax layers. More than 26000 parameters are extracted from the dataset.

to higher activation regions. The filters are also activated by specific bands in channels, in a more located way, such as in row 2, column 6.

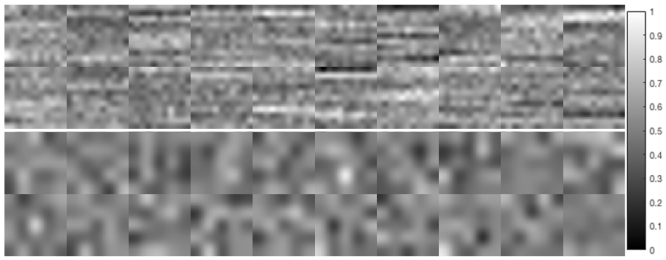

Fig. 4. First 20 filter weights in the first and second convolutional layers after training.

The classification assessment was measured by the correct classification rate and how close it was to the maximum rate (100%). The observation of the accuracy rate in contrast with the accuracy achieved by chance, the so called chance-level rate, is common in neural signal processing [22], [23].

The theoretical chance-level rates for groups 1 and 2 and group 3 are 50% and 25%, respectively. These measurements consider an infinite sample size scenario, where the relation $100/c$ is true (being c the number of classes), which is unfeasible for real applications. For actual scenarios, [24] propose the use of binomial inverse cumulative distribution function to compute the statistically significant threshold of the classification, assuming that the classification errors obey a binomial cumulative distribution.

Following the [24] proposal and assuming the binomial cumulative distribution, our data chance-level rate is $St(\alpha) = 25.30$, for four classes ($c = 4$) and $\alpha = 0.001$, being α the ratio of tolerated false positives. This threshold indicates that at least 25.30% of samples were predicted by chance, similar to the theoretical measure. Taking the same α, and isolating the targets in terms of left/right and up/down, the thresholds $St(\alpha) = 50.42$ and $St(\alpha) = 50.50$, must be overcomed.

On the other hand, it is possible to measure the statistical significance of classification using permutation tests [25]. In these non-parametric tests the samples are permuted across classes and the classification accuracy is measured. The binomial method requires minimal assumptions for validity, the permutation method, in turn, provides a flexible and intuitive approach to assess the correct classification.

In our data, the classes were permuted among the samples and the randomization tests are pictured in figures 5a-5c of section III-A. Given the classes distribution, 85% of the samples were randomized.

III. Results

All the experiments reported in this work were run on a 2.7GHz Intel Core i7-7500U with 16GB of RAM and NVIDIA GeForce 940M 4GB graphic card. Both train and test sets were processed by CUDA kernels. On average, the training time of one CNN model - for groups 1 and 2 - was approximately 5 hours to converge. Considering the batch size of 128 samples, on average, 12 iterations were necessary to process the data at each epoch, on a total of 20 epochs. The training time of one CNN model for group 3 was 10 hours, by keeping the same number of epochs as before and it took 30 iterations to process the data in batches. It is important to stress that until the final CNN architecture was reached, we performed experiments during four weeks and tested several parameters to fine tune the CNN architecture described in this work.

A. Overall Classification Performance of Reaching Targets

To evaluate the overall performance of the CNN classifiers in predicting reaching targets before movement onset, we trained and tested their accuracy on experimental data of the 10 days (we call them overall classifiers) and arranged the four classes into three different groups. More specifically, four CNN classifiers were trained for predicting left and right targets (group 1), four CNN for predicting up and down targets (group 2) and four to predict left, right, up, and down targets (group 3). All the twelve CNN classifiers were trained with 2D images as described in Section II-B.

Figures 5a, 5b and 5c show the mean and standard deviation (shaded area) accuracy results of the test set from $-2,25s$ to $0s$, respectively. We observed that all the three classification performances demonstrated similar curve shapes. They increased from chance level around $-1s$ and achieved a peak performance before movement onset at $-382.8ms$. This time yielded the highest mean accuracies for all three classifications: (69.06 ± 0.33), (65.33 ± 0.94) and (50.34 ± 0.38).

B. Day Specific Classifier Performance

To evaluate daily classification performance and analyze if the subject's neural signatures improves their discrimination power over day sessions, we trained 10 CNN classifiers with data from that day, that is, the day 1 classifier was trained with data of the first day and so on. This analysis is challenging because the onset of visually-guided self-paced reaching is subjected to more sources of errors compared to cue-based experiments. For example, mocap error due to calibration problems, the subject requires more concentration to perform gaze-centered reaching and muscular fatigue because he performs reaching movements while standing. Because group 3 gave the lower performance compared to the other groups

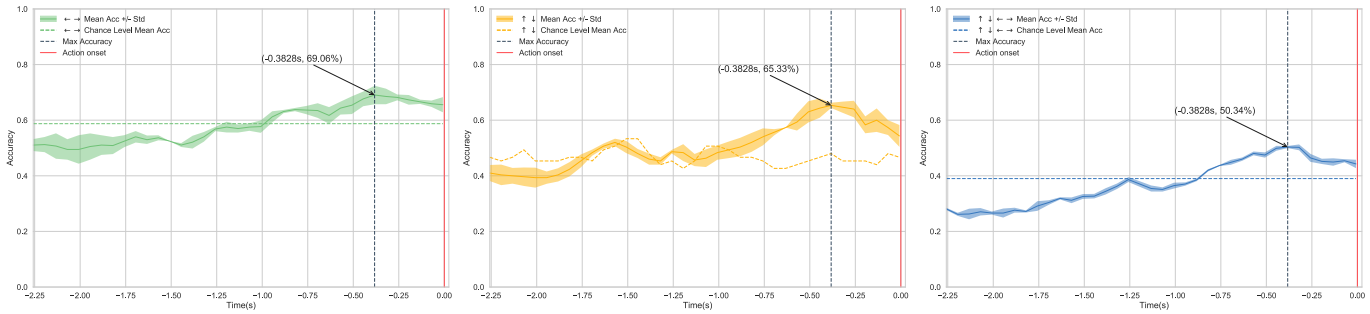

(a) Classification performance for group 1 (b) Classification performance for group 2 (c) Classification performance for group 3

Fig. 5. Classification accuracy of the test .The horizontal dotted lines are the chance level computed for each group. The best mean accuracy and the time where they occur is shown by the vertical dotted line in each Figure.

(see Figure 5), it was analyzed. Table I depicts the maximum accuracy and anticipation time for each acquisition day.

TABLE I
THIS TABLE SHOWS THE MAXIMUM CLASSIFICATION ACCURACY (COLUMN 2) FOR EACH DAY (COLUMN 1) AND THE TIME BEFORE REACHING ONSET (COLUMN 3).

Day	Max Accuracy (%)	Anticipation Time (ms)
1	56.00	382
2	47.82	272
3	50.00	944
4	57.14	507
5	52.38	444
6	**61.90**	**757**
7	52.17	257
8	57.89	1569
9	40.00	1132
10	61.90	781

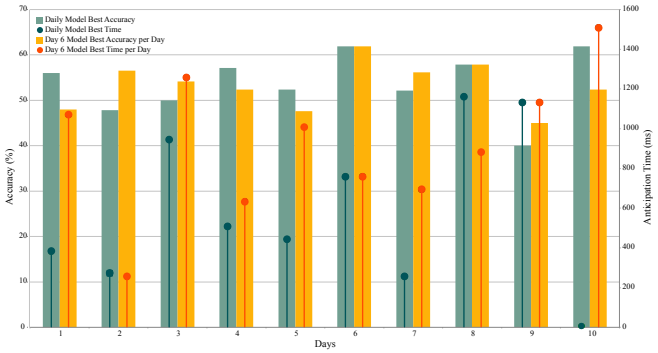

Fig. 6. Comparison of classification performance between day specific and selected classifiers. The bars and stems refer to the accuracy and anticipation time, respectively.

C. Selected Classifier Performance

In order to decode EEG patterns that were corrupted by some source of noise and improve the classification performance of reaching targets, we selected to test the day specific classifier that gave the highest accuracy before movement onset. Our assumption is that, this classifier was able to learn the most relevant patterns encoded in the images built from that day. From Table I the test classifier was built with the day 6 training data set. Figure 6 shows the classification performance of applying the selected classifier on the test set of each specific day. We can observe that it was able to improve the classification accuracy of the day 9 above chance level. This confirms our assumption that training a classifier with relevant features can track neural signatures associated with reaching targets in the presence of noise.

IV. Discussions and Conclusion

We have presented a new approach for classification of reaching targets before movement onset. In our approach, we combined the discriminant power of EEG images with the feature extraction capabilities of a deep learning technique called Convolutional Neural Network (CNN), which is suitable to learn patterns directly from image data and flexible enough to overcome local distortions. We have proposed the use of images built from the temporal amplitudes of 8 frequency components filtered from the δ band, because this brain rhythm is suitable for the analysis of anticipatory movements. The CNN classifiers were trained with images from short epochs of 250ms within the intention period of 1s before reaching onset. We then used a sliding window technique to continuously classify the intended target. This allowed us to visualize the temporal classification evolution of visually-guided reaching in 3D space before movement onset. We demonstrated the performance of our approach in several situations as described in Section III.

Regarding overall classification (Section III-A). Noticeably, the CNN classifiers performed better for left and right targets when compared to the up and down targets and even better than group 3. The later is probably a consequence of the increasing in the number of classes. On the other hand, the difference in performance for groups 1 and 2 can be a consequence of a sensorimotor reference frame transformation used in visually-guided reaching in 3D space, that are performed in the brain to transform visual signals into a motor plan to guide the arm towards the targets [5]. During the left and right reaching, the subject turned his head to gaze-center left or right targets, enforcing brain signals to take account of this

transformation. On the opposite, up and down targets did not required head motions. These results suggest that the visual selection of reaching targets can be discriminated using neural signatures from temporal amplitudes of δ components encoded within images.

Regarding daily classification (Section III-B). The results suggest that building a model in a daily basis in most cases provided better results than merging data from all days. Despite days 2 and 9 loss in performance, the other days have shown a significant increase in accuracy when compared to the best result depicted in Figure 5c. An increase in anticipation time can also be observed for the majority of the days. The lowest performance of the day 9 classifier may indicate that the neural signatures were corrupted by noise because the maximum classification performance was at chance level. As a consequence, the day 9 classifier was unable to efficiently learn target patterns associated to reaching intentions within our EEG images.

We can draw several conclusions from Figure 6 (Section III-C). Regarding classification performance, in four of the nine days the accuracy has raised. Regarding time anticipation earlier detection happened on six of the nine days. We also noticed that days 1, 4, 5, 7 and 10 had a small decrease in accuracy performance, but regarding earlier detection the test classifier did it earlier than day specific classifiers. On the other hand, regarding accuracy results of days 2 and 9, we observed an increase in classification of the selected classifier than day specific classifiers. By turning our attention to the specific day and overall classifiers, the classification performance of the selected classifier on the overall training set was 44.16% at the time $-687ms$, which gives a decreasing in performance of only 6.18%. Nevertheless, the best classification result is still above chance level and it occurred earlier.

Overall, the proposed approach has shown the feasibility of building EEG images from temporal amplitudes of EEG signals, to discriminate the direction of targets in 3D space before movement onset. This may has important applications in the control of neuro-prophetesses of brain-computer interfaces, such as the premature decoding of arm trajectories during visually-guided reaching in 3D space. Finally, our results open the opportunity for a new field in the use of decoded EEG images for VR applications.

ACKNOWLEDGMENT

This work was supported by the CNPq projects N° 482685/2012-3, 443304/015-7, 440880/2013-0, 310468/2014-0 and 420801/2016-2. This work was also partially supported by the swiss SNF project N° 200021_140910.

REFERENCES

[1] G. Pfurtscheller, S. Reinhold, and R. Scherer, "Brain-Computer Interfaces used for Virtual Reality Control," *ICABB 2010 : 1st International Conference on Applied Bionics and Biomechanics*, no. 27731, pp. 3–21, 2010. [Online]. Available: http://www.brainable.org/Documents/PfurtschellerG-ICABB.pdf

[2] a. Lécuyer, F. Lotte, R. Reilly, and R. Leeb, "Brain-computer interfaces, virtual reality, and videogames." *IEEE Computer*, 2008. [Online]. Available: http://www.tara.tcd.ie/bitstream/handle/2262/32127/Brain-Computer+Interfaces.pdf?sequence=1

[3] I. Iturrate, R. Chavarriaga, L. Montesano, J. Minguez, and J. D. R. Millán, "Teaching brain-machine interfaces as an alternative paradigm to neuroprosthetics control." *Scientific reports*, vol. 5, p. 13893, 2015. [Online]. Available: http://www.nature.com/srep/2015/150910/srep13893/full/srep13893.html

[4] E. Y. L. Lew, R. Chavarriaga, S. Silvoni, and J. D. R. Millán, "Single trial prediction of self-paced reaching directions from EEG signals." *Frontiers in neuroscience*, vol. 8, pp. 1–13, Jan. 2014.

[5] G. Blohm, G. P. Keith, and J. D. Crawford, "Decoding the cortical transformations for visually guided reaching in 3d space," *Cerebral Cortex*, vol. 19, no. 6, p. 1372, 2009.

[6] G. Garipelli, R. Chavarriaga, and J. D. R. Millán, "Single trial analysis of slow cortical potentials: a study on anticipation related potentials," *Journal of Neural Engineering*, vol. 10, no. 3, p. 036014, 2013.

[7] G. Pfurtscheller and C. Neuper, "Motor imagery and direct brain-computer communication," *Proceedings of the IEEE*, vol. 89, no. 7, pp. 1123–1134, Jul. 2001.

[8] P. S. Hammon, S. Makeig, H. Poizner, E. Todorov, and V. R. de Sa, "Predicting Reaching Targets from Human EEG," *Signal Processing Magazine, IEEE*, vol. 25, no. 1, pp. 69–77, 2008. [Online]. Available: http://dx.doi.org/10.1109/msp.2008.4408443

[9] H. Cecotti and A. Grser, "Convolutional neural networks for p300 detection with application to brain-computer interfaces." *IEEE Trans. Pattern Analysis Machine Intelligence*, vol. 33, no. 3, pp. 433–445, 2011.

[10] X. An, D. Kuang, X. Guo, Y. Zhao, and L. He, "A deep learning method for classification of eeg data based on motor imagery." in *Intelligent Computing in Bioinformatics*, ser. Lecture Notes in Computer Science, vol. 8590. Springer, 2014, pp. 203–210.

[11] Y. Tabar and U. Halici, "A novel deep learning approach for classification of eeg motor imagery signals," *Journal of Neural Engineering*, vol. 14, no. 1, 2017.

[12] E. Molla and R. Boulic, "Singularity Free Parametrization of Human Limbs," in *Proceedings of Motion on Games - MIG '13*. New York, New York, USA: ACM Press, 2013, pp. 187–196.

[13] Y. Renard, F. Lotte, G. Gibert, M. Congedo, E. Maby, V. Delannoy, O. Bertrand, and A. Lcuyer, "Openvibe: An open-source software platform to design, test, and use braincomputer interfaces in real and virtual environments," *Presence: Teleoperators and Virtual Environments*, vol. 19, no. 1, pp. 35–53, 2010.

[14] J. Wolpaw and C. Boulay, "Brain signals for brain-computer interfaces," in *Brain-Computer Interfaces*, ser. The Frontiers Collection, B. Graimann, G. Pfurtscheller, and B. Allison, Eds. Springer Berlin Heidelberg, 2010, pp. 29–46.

[15] S. W. Smith, *The Scientist and Engineer's Guide to Digital Signal Processing*. San Diego, CA, USA: California Technical Publishing, 1997.

[16] S. J. Luck, "An introduction to the event-related potential technique," 2014.

[17] G. Garipelli, R. Chavarriaga, and J. R. Milln, "Single Trial Recognition of Anticipatory Slow Cortical Potentials: The Role of Spatio-Spectral Filtering," in *Proceedings of the 5th International Conference on Neural Engineering*, ser. International IEEE EMBS Conference on Neural Engineering. IEEE, 2011.

[18] Y. LeCun, L. Bottou, Y. Bengio, and P. Haffner, "Gradient-based learning applied to document recognition," in *Proceedings of the IEEE*, vol. 86, no. 11, 1998, pp. 2278–2324.

[19] S. Min, B. Lee, and S. Yoon, *Deep learning in bioinformatics*. Oxford University Press, 2016, p. 42.

[20] X. Glorot, A. Bordes, and Y. Bengio, "Deep sparse rectifier neural networks," in *Proceedings of the Fourteenth International Conference on Artificial Intelligence and Statistics (AISTATS-11)*, G. J. Gordon and D. B. Dunson, Eds., vol. 15. Journal of Machine Learning Research - Workshop and Conference Proceedings, 2011, pp. 315–323.

[21] V. Nair and G. E. Hinton, "Rectified linear units improve restricted boltzmann machines." in *ICML*, J. Frnkranz and T. Joachims, Eds. Omnipress, 2010, pp. 807–814.

[22] M. Ahn, S. Ahn, J. H. Hong, H. Cho, K. Kim, B. S. Kim, J. W. Chang, and S. C. Jun, "Gamma band activity associated with bci performance: simultaneous meg/eeg study," *Frontiers in Human Neuroscience*, vol. 7, p. 848, 2013.

[23] I. Momennejad and J.-D. Haynes, "Human anterior prefrontal cortex encodes the what and when of future intentions," *NeuroImage*, vol. 61, no. 1, pp. 139 – 148, 2012.

[24] E. Combrisson and K. Jerbi, "Exceeding chance level by chance: The caveat of theoretical chance levels in brain signal classification and statistical assessment of decoding accuracy," *Journal of Neuroscience Methods*, vol. 250, pp. 126 – 136, 2015, cutting-edge {EEG} Methods.
[25] T. E. Nichols and A. P. Holmes, "Nonparametric permutation tests for functional neuroimaging: A primer with examples. human brain mapping," *Human brain mapping*, vol. 15, no. 1, pp. 1–25, 2001.